Saudi Pharmaceutical Journal 32 (2024) 102055

HOSTED BY

Contents lists available at ScienceDirect

Saudi Pharmaceutical Journal

journal homepage: www.sciencedirect.com

Pharmacological p38 MAPK inhibitor SB203580 enhances AML stem cell line KG1a chemosensitivity to daunorubicin by promoting late apoptosis, cell growth arrest in S-phase, and miR-328-3p upregulation

Sara Bahattab [a,b,1], Ali Assiri [a,c,1], Yazeid Alhaidan [d], Thadeo Trivilegio [e], Rehab AlRoshody [a], Sarah Huwaizi [e], Bader Almuzzaini [d], Abir Alamro [b], Manal Abudawood [c], Zeyad Alehaideb [d], Sabine Matou-Nasri [a,f,*]

[a] Blood and Cancer Research Department, King Abdullah International Medical Research Center (KAIMRC), King Saud bin Abdulaziz University for Health Sciences (KSAU-HS), Ministry of National Guard-Health Affairs (MNG-HA), Riyadh 11481, Saudi Arabia
[b] Biochemistry Department, College of Science, King Saud University, Riyadh 11451, Saudi Arabia
[c] Department of Clinical Laboratories Sciences, College of Applied Medical Sciences, King Saud University, Riyadh 11362, Saudi Arabia
[d] Medical Genomics Research Department, KAIMRC, KSAU-HS, MNG-HA, Riyadh 11481, Saudi Arabia
[e] Medical Research Core Facility and Platforms, KAIMRC, KSAU-HS, MNG-HA, Riyadh 11481, Saudi Arabia
[f] Biosciences Department, Faculty of the School of Systems Biology, George Mason University, Manassas, VA 20110, United States

ARTICLE INFO

Keywords:
Acute myeloid leukemia
Daunorubicin
p38 MAPK inhibitor
SB203580
Apoptosis
miR-328-3p

ABSTRACT

Acute myeloid leukaemia (AML) is characterized by uncontrolled proliferation of myeloid progenitor cells and impaired maturation, leading to immature cell accumulation in the bone marrow and bloodstream, resulting in hematopoietic dysfunction. Chemoresistance, hyperactivity of survival pathways, and miRNA alteration are major factors contributing to treatment failure and poor outcomes in AML patients. This study aimed to investigate the impact of the pharmacological p38 mitogen-activated protein kinase (MAPK) inhibitor SB203580 on the chemoresistance potential of AML stem cell line KG1a to the therapeutic drug daunorubicin (DNR). KG1a and chemosensitive leukemic HL60 cells were treated with increasing concentrations of DNR. Cell Titer-Glo®, flow cytometry, phosphokinase and protein arrays, Western blot technology, and reverse transcription-quantitative polymerase chain reaction (RT-qPCR) were employed for assessment of cell viability, half-maximal inhibitory concentration (IC_{50}) determination, apoptotic status detection, cell cycle analysis, apoptosis-related protein and gene expression monitoring. Confocal microscopy was used to visualize caspase and mitochondrial permeability transition pore (mPTP) activities. Exposed at various incubation times, higher DNR IC_{50} values were determined for KG1a cells than for HL60 cells, confirming KG1a cell chemoresistance potential. Exposed to DNR, late apoptosis induction in KG1a cells was enhanced after SB203580 pretreatment, defined as the combination treatment. This enhancement was confirmed by increased cleavage of poly(ADP-ribose) polymerase, caspase-9, caspase-3, and augmented caspase-3/-7 and mPTP activities in KG1a cells upon combination treatment, compared to DNR. Using phosphokinase and apoptosis protein arrays, the combination treatment decreased

Abbreviations: ALL, acute lymphoblastic leukemia; AML, acute myeloid leukemia; Bcl-2, B-cell lymphoma 2; Becton Dickinson, BD; cAMP, cyclic adenosine monophosphate; CDKN, cyclin-dependent kinase inhibitor; cDNA, complementary DNA; CREB, cAMP response element-binding; DMSO, dimethyl sulfoxide; DNR, daunorubicin; FACS, fluorescence-activated cell sorting; FADD, Fas-associated death domain; FBS, fetal bovine serum; FITC, fluorescein isothiocyanate; FLT3, fms-like tyrosine kinase 3; GAPDH, glyceraldehyde 3-phosphate dehydrogenase; HSP, heat shock protein; IAP, inhibitor of apoptosis protein; IC_{50}, half-maximal inhibitory concentration; ITD, internal tandem duplication; MAPK, mitogen-activated protein kinase; miRNA, micro-ribonucleic acid; mPTP, mitochondrial permeability transition pore; mRNA, messenger RNA; MSK, mitogen- and stress-protein kinase; mTOR, mammalian target of rapamycin; PARP, poly(ADP-ribose) polymerase; PBS, phosphate-buffered saline; PI, propidium iodide; PI3K, phosphatidylinositol 3-kinase; PYK, proline-rich tyrosine kinase; RPMI, Roswell Park Memorial Institute; RSK, ribosomal S6 kinase; RT-qPCR, reverse transcription-quantitative polymerase chain reaction; SD, standard deviation; SMAC, second mitochondria-derived activator of caspases; STAT, signal transducer and activator of transcription; STS, staurosporine; TNFR, tumor necrosis factor receptor; TP53, tumor protein p53; TRAIL-R, TNF-related apoptosis inducing ligand-receptor.

* Corresponding author at: King Abdullah International Medical Research Center, Ministry of National Guard-Health Affairs, P.O. Box 22490, Riyadh 11426, Saudi Arabia.
E-mail address: matouepnasrisa@mngha.med.sa (S. Matou-Nasri).
[1] Contributed equally to this work.

https://doi.org/10.1016/j.jsps.2024.102055
Received 26 February 2024; Accepted 27 March 2024
Available online 30 March 2024

survival Akt phosphorylation and anti-apoptotic Bcl-2 expression levels in KG1a cells while increasing the expression levels of the tumor suppressor p53 and cyclin-dependent kinase inhibitor p21, compared to DNR. Cell cycle analysis revealed KG1a cell growth arrest in G2/M-phase caused by DNR, while combined treatment led to cell growth arrest in S-phase, mainly associated with cyclin B1 expression levels. Remarkably, the enhanced KG1a cell sensitivity to DNR after SB203580 pretreatment was associated with an increased upregulation of miR-328-3p and slight downregulation of miR-26b-5p, compared to DNR effect. Altogether, these findings could contribute to the development of a new therapeutic strategy by targeting the p38 MAPK pathway to improve treatment outcomes in patients with refractory or relapsed AML.

1. Introduction

Acute myeloid leukemia (AML), a blood cancer characterized by excessive proliferation and blocked maturation of myeloid progenitor cells, leads to accumulation of non-functional blood cells in the bone marrow and bloodstream, resulting in hematopoietic failure (*i.e.*, anemia, thrombocytopenia, or granulocytopenia) (Jäger et al., 2021; Trino et al., 2022). Several risk factors such as aging, family tumor history, hepatitis B or C virus infection, radiation and environmental exposure cause abnormal genetic and chromosomal alterations in hematopoietic stem and progenitor cells, which trigger hyperactivation of survival pathways and receptor tyrosine kinase-RAS signaling, leading to AML pathogenesis (Nepstad et al., 2020; Kishtagari and Levine, 2021; Guo et al., 2022). AML is the most common acute malignant hematologic disorder in adults. Cytogenetic and genomic characterizations contributing to AML classification into subgroups, as well as the establishment of clinical risk profile and the stratification of AML patients are revealed to be crucial for prognosis and tailored treatment (Isidori et al., 2019; Hou and Tien, 2020; Boscaro et al., 2023). In clinical practice, various modalities of AML treatment are employed, which are commonly drug-based protocols, including standard first-line chemotherapy, targeted therapy, antibody-drug conjugates, hypomethylating agents, and small molecule tyrosine kinase inhibitors (Miyamoto et al., 2022; Récher et al., 2022). In severe aggressive forms of AML, consolidative allogeneic stem cell transplantation is mainly recommended (Jovein et al., 2023). Patients under 60 have a two-thirds survival probability, while patients over 60, tolerating less AML treatment, have a poorer prognosis with only a one-third survival probability over 3 years (Vakiti and Mewawalla, 2023). Generally, AML is lethal within a few weeks of diagnosis if left untreated. The standard chemotherapy drugs are idarubicin or cytarabine combined with daunorubicin (DNR), an anthracycline topoisomerase inhibitor, which has been the most frequently used efficacy and safety drug for AML remission by induction therapy (Wang et al., 2020). Even when complete remission is achieved, approximately 70 % of AML patients relapse within five years due to minimal residual disease (Levin et al., 2021; Tiong and Loo, 2023). Clinical studies have revealed that minimal residual disease and chemotherapeutic drug resistance are considered the main causes of AML treatment failure (Levin et al., 2021; Tiong and Loo, 2023; Stelmach and Trumpp, 2023).

Tumor chemoresistance is classified as a primary, adaptive or acquired process (Lei et al., 2023; Niu et al., 2022). Primary drug resistance refers to refractories caused by the non-proliferative G_0 phase of leukemic cells, which therefore do not respond to treatments (Zhang et al., 2019). On the other hand, acquired resistance, also known as secondary resistance, occurs after receiving induction therapy, during which initially reactive tumor cells become resistant to the treatment due to genetic mutations (Zhang et al., 2019). Several clinical studies have suggested the contribution of multidrug-resistant AML stem cell population as a main factor leading to the relapse of AML patients, which raises the mortality rate (van Gils et al., 2021; Fajardo-Orduña et al., 2021). Therefore, targeting this chemoresistant AML cell subpopulation, which predominantly exhibits stemness characteristics, could potentially improve the treatment response of relapsed disease and enhance overall survival rates of AML patients (Khaldoyanidi et al., 2022; Huang et al., 2023). Different factors contribute to the resistance mechanism, such as drug inactivation or alteration, tumor microenvironment, activation of compensatory survival pathways, including phosphatidylinositol 3-kinase (PI3K)/Akt/mammalian target of rapamycin (mTOR), and dysregulated micro(mi)RNAs (Gabra and Salmena, 2017; Darici et al., 2020; Ganesan et al., 2022; Lei et al., 2023). Among the various therapeutic strategies in development, targeting the survival p38 mitogen-activated protein kinase (MAPK) pathway, responsible for miRNA alterations, has become of great interest to sensitize cancer stem cells to chemotherapy (Antoon et al., 2013; Kudaravalli et al., 2022). We previously reported the improved sensitivity of AML stem cell line KG1a to 5-Fluorouridine after blocking p38 MAPK using the pharmacological inhibitor SB202190, associated with upregulation of miR-328-3p (Matou-Nasri et al., 2022). In this study, presented as a promising therapeutic strategy for relapsed AML patients, we evaluated the drastic reduction in the chemoresistance potential of AML stem KG1a cells upon pretreatment with the pharmacological p38 MAPK inhibitor SB203580 followed by the addition of DNR. The resulting cell death was investigated extensively using apoptosis-related assays, cell cycle analysis, and by monitoring cell death-related proteins, genes and miRNAs expression levels.

2. Materials and methods

2.1. Reagents

All reagents were purchased from Thermo Fisher Scientific (Waltham, MA, USA) unless indicated otherwise.

2.2. AML cell culture and treatment

The human AML stem cell line KG1a (#CCL-246.1) and the promyelocytic leukemia cell line HL60 (#CCL-240) were obtained from the American Type Culture Collection (Manassas, VA, USA). Both cell lines were grown in complete Roswell Park Memorial Institute (RPMI 1640) medium (Gibco®) supplemented with 10 % heat-inactivated fetal bovine serum (FBS), 100 U/ml penicillin – 100 µg/ml streptomycin solution and 2 mM L-glutamine and cultured at 37 °C in a saturated air humidity 5 % CO_2-incubator.

The cells were exposed to various concentrations (0.05–10 µM) of DNR (#sc-200921, Santa Cruz Biotechnology, Dallas, TX, USA) at different incubation times. The cell pretreatment with 20 µM pharmacological p38 MAPK inhibitor SB203580 (#sc-3533A, Santa Cruz Biotechnology) was carried out 2 h prior to DNR addition corresponding to the combination treatment, experimental conditions defined from pilot studies. Dimethyl sulfoxide (DMSO), solvent used for DNR and SB203580 reconstitutions, was used as a negative control while staurosporine (STS, #sc-3510B, Santa Cruz Biotechnology), a strong protein kinase inhibitor, was used as a positive control.

2.3. Cell viability assay

Both KG1a and HL60 cells (2.5×10^4 cells/well) were seeded in an opaque 96-well plate (Greiner®). After various times of incubation (24, 48 and 72 h), the cell viability was assessed using CellTiter-Glo® Luminescent Cell Viability Assay (Promega, Madison, WI, USA)

according to manufacturer's instructions. This assay measures the amount of ATP generated, which serves as an indicator of viable cells. Briefly, the CellTiter-Glo® reagent (100 µl) was added to each well, mixed on an orbital shaker for 2 min, and then incubated for 10 min at room temperature, protected from light. The luminescent signal was recorded using an EnVision microplate reader (PerkinElmer, Waltham, MA, USA). The half-maximal inhibitory concentration (IC_{50}) of DNR resulting in a 50 % decrease in cell viability was determined by a sigmoidal dose–response (non-linear regression) curve using Excel.

2.4. Flow cytometry

The cell cycle was analyzed using the Becton Dickinson (BD) Cycletest Plus DNA Reagent Kit (#340242, BD Biosciences, Franklin Lakes, NJ, USA) according to the manufacturer's instructions. Briefly, KG1a cells were collected after 72 h of incubation and then washed three times with buffer solution. Next, the cells were suspended in a fixative solution A (250 µl), mixed gently, and incubated for 10 min at room temperature. Then, to permeabilize the cell membranes, the solution B (200 µl) was added, mixed gently, and incubated for 10 min at room temperature. Finally, to stain the DNA, the solution C (200 µl) was added, mixed gently, and incubated on ice in the dark for 10 min. The cells (10,000) were then analyzed on a FACScanto II flow cytometer (BD Biosciences) using Kaluza software (Beckman Coulter Inc.).

Apoptosis status was determined using the fluorescein isothiocyanate (FITC) Annexin V Apoptosis Detection Kit with propidium iodide (PI, #640914, BioLegend, San Diego, CA, USA). Briefly, the cells were collected, washed with phosphate-buffered saline (PBS), and suspended in 1 × binding buffer (100 µl). Then, Annexin V and PI solutions (5 µl) were added and incubated for 15 min in the dark. The cells (10,000) were then analyzed on a FACScanto II flow cytometry system (BD Biosciences) using Diva software, where Annexin V/PI (−/−), Annexin V/PI (+/−), Annexin V/PI (+/+), and Annexin V/PI (−/+) indicate healthy cells, early apoptosis, late apoptosis, and necrosis, respectively.

2.5. Confocal fluorescence microscopy

Caspase-3/-7 and mitochondrial permeability transition pore (mPTP) activities were assessed using Image-iT LIVE Red Caspase-3/-7 detection kit and Image-iT™ LIVE Mitochondrial Transition Pore Assay kit (Molecular Probes, Eugene, OR, USA) as previously described (Matou-Nasri et al., 2022).

2.6. Western blot technology

From protein extraction, quantitation, separation by 12 % sodium dodecyl sulfate–polyacrylamide gel electrophoresis, transfer to polyvinylidene fluoride membrane, and to protein visualization, Western blot technology was employed as previously described (Matou-Nasri et al., 2022). Diluted in blocking buffer, the primary antibodies used were rabbit anti-cleaved caspase-3 (#9664, dilution 1:1000), pro-caspase 3 (#9665, 1:1000), cleaved caspase-9 (#9505, 1:1000), cleaved poly (ADP-ribose) polymerase (PARP) (#5625, 1:500), PARP (#9542, 1:500), mouse pro-caspase-9 (#9508, 1:1000) monoclonal antibodies provided by Cell Signaling Technology (Danvers, MA, USA), and mouse anti-cyclin A (#sc-271645, 1:1000), cyclin B1 (#sc-70898, 1:1000), cyclin D1 (#sc-8396, 1:1000) monoclonal antibodies purchased from Santa Cruz Biotechnology, and mouse anti-glyceraldehyde 3-phosphate dehydrogenase (GAPDH) monoclonal antibody (#AM4300, 1:5000) from Invitrogen.

2.7. Phosphokinase and apoptosis-related protein arrays

Kinase phosphorylation and apoptosis-related protein expression levels were detected in KG1a cell lysates using the Proteome Profiler Human Phospho-Kinase (#ARY003B, R&D Systems, Minneapolis, MN, USA) and Apoptosis (#ARY009, R&D Systems) Array kits according to the manufacturer's instructions. The luminescent signal was visualized on the C-Digit® Imaging System (LI-COR Biosciences, Lincoln, NE, USA). Protein expression level was quantified using ImageJ software (https://rsbweb.nih.gov/ij/index.htmL).

2.8. Reverse transcription-quantitative polymerase chain reaction (RT-qPCR)

Whole RNA was extracted using RNeasy Mini Kit (QIAGEN, Hilden, Germany) according to the manufacturer's instructions. The complementary DNA (cDNA) synthesis was carried out using the high-capacity cDNA reverse transcription kit (cat# 4368814) following the manufacturer's instructions. Briefly, total RNA extract (1000 ng) was transferred to a clean 0.2 ml PCR tube, and the volume was adjusted to 10 µl with nuclease-free water. Then, the reverse transcription master mix (10 µl) was added to each sample. The tubes were tightly sealed and subjected to thermal cycling as instructed. The resulting cDNA was stored at −20 °C until use. For RT-qPCR, the total reaction mixture (10 µl) included 25 ng of cDNA (in 4.5 µl), 5 µl of the PowerUp SYBR Green Master Mix (#A25742, Applied Biosystems), and 0.5 µl of a mixed forward and reverse primer solution (10 µM). Each sample was performed in triplicate to ensure the accuracy and reproducibility of the results. Real-time PCR was performed on the Applied Biosystem™ QuantStudio 6 Flex system (Thermo Fisher Scientific) using the following parameters: an initial step at 95 °C for 10 min, followed by 40 cycles of amplification at 95 °C for 15 sec and 60 °C for 1 min. The targeted genes and the primers sequences employed are summarized in Table 1.

Regarding the monitoring of miRNA expression level, cDNA templates were synthesized using the TaqMan Advanced miRNA cDNA synthesis kit (#A28007, Applied Biosystems) according to the manufacturer's instructions. To assess the expression levels of miR-26b-5p, miR-328-3p, and the endogenous control gene miR-361-5p, predesigned Advanced miRNA assays (Applied Biosystems) were utilized. These assays were used in conjunction with the TaqMan Fast Advanced Master Mix (Applied Biosystems) for real-time PCR analysis. Real-time PCR was performed on the Applied Biosystem™ QuantStudio 6 Flex system (Thermo Fisher Scientific) using the following parameters: an initial step at 95 °C for 20 sec, followed by 40 cycles of amplification at 95 °C for 1 sec and 60 °C for 20 sec. The sequences of the mature miRNAs and the ID of the TaqMan Advanced miRNA assays are indicated in Table 2.

2.9. Statistical analysis

Data are expressed as mean ± standard deviation (SD) from three independent experiments. One-way ANOVA followed by a post-hoc Tukey test was used to determine the statistical significance for comparison of two groups. A value of p less than 0.05 was considered significant.

3. Results

3.1. AML stem cell KG1a chemoresistance potential to daunorubicin (DNR)

The viability of KG1a and HL60 cells was assessed using the CellTiter-Glo® method after cell exposure to increasing DNR concentrations (0.05–10 µM) for different incubation times (24, 48, and 72 h). Compared to untreated cells (i.e., control), corresponding to 100 %, 0.1–1 % DMSO did not affect the viability of HL60 and KG1a cells, while kinase inhibitor STS at 0.1 µM and 1 µM decreased HL60 and KG1a cell viability by 45 and 90 % after 24–48 and 72 h of incubation, respectively (Fig. 1). Increasing DNR concentrations resulted in decreased HL60 cell viability (Fig. 1A) with IC_{50} values determined to be 0.157 µM, 0.107 µM, and 0.053 µM of DNR, and KG1a cell viability (Fig. 1B) with DNR

Table 1
Apoptosis-related gene primer sequences for RT-qPCR.

Gene	Forward primer sequence (5′-3′)	Reverse primer sequence (5′-3′)
TP53	GAGATGTTCCGAGAGCTGAATGAGGC	TCTTGAACATGAGTTTTTTATGGCGGGAGG
BAX	GATGCGTCCACCAAGAAG	AGTTGAAGTTGCCGTCAG
BCL-2	AAGATTGATGGGATCGTTGC	GCGGAACACTT GATTCTGGT
BCL-xL	CCCAGAAAGGATACAGCTGG	GCGATCCGACTCACCAATAC
Cyclin A	GTCACCACATACTATGGACATG	AAGTTTTCCTCTCAGCACTGAC
Cyclin D1	ACAAACAGATCATCCGCAAACAC	TGTTGGGGCTCCTCAGGTTC
CDKN1A	GCGATGGAACTTCGACTTTGT	GGGCTTCCTCTTGGAGAAGAT
GAPDH	TGATGACATCAAGAAGGTGGTGAAG	TCCTTGGAGGCCATGTGGGCCAT

Table 2
miRNA TaqMan primer sequences and assays ID.

miRNA	Mature miRNA sequence (5′-3′)	TaqMan Advanced miRNA assays ID (Applied Biosystems)
miR-26b-5p	UUCAAGUAAUUCAGGAUAGGU	478418_mir
miR-328-3p	CUGGCCCUCUCUGCCCUUCCGU	478028_mir
miR-361-5p	UUAUCAGAAUCUCCAGGGGUAC	478056_mir

IC_{50} values of approximately 1.3 μM, 0.9 μM, and 0.7 μM after 24, 48, and 72 h of incubation, respectively; which confirmed the chemoresistance potential of KG1a cells to DNR (Fig. 1).

3.2. KG1a cell pretreatment with SB203580 enhanced DNR-induced late apoptosis

Based on a previous study, blocking the p38 MAPK pathway with the pharmacological inhibitor SB202190 resulted in enhanced sensitivity of KG1a cells to the chemotherapeutic drug 5-Fluorouridine, leading to increased induction of apoptosis (Matou-Nasri et al., 2022). In the present study, the impact of another pharmacological p38 MAPK inhibitor (*i.e.*, SB203580) on KG1a and HL60 cells exposed to the conventional chemotherapeutic drug suitable for AML patients (*i.e.*, DNR) was investigated on cell death processes, including a comprehensive analysis of the apoptosis and the cell cycle in KG1a cells. Thus, after 72 h of incubation, the apoptotic status was first determined using fluorescence-activated cell sorting (FACS) analysis following Annexin V/PI double staining. Compared to untreated highly viable cells (*i.e.*, control), HL60 cells exposed to 0.05–0.09 μM DNR underwent apoptosis and the entire DNR-treated cell population shifted to late apoptosis after SB203580 pretreatment (Supplementary Fig. 1). Concerning KG1a cell apoptotic status, representative scatter plots are shown in Fig. 2A. DNR tested at 0.7 μM (IC_{50} for 72 h of incubation) led to approximately 31.5 % decrease in percentage of viable cells and increased the percentage of apoptotic cells by ~30 % ($p < 0.05$), compared to the control (Fig. 2B). The combined treatment of KG1a cells, corresponding to SB203580 pretreatment followed by DNR addition, resulted in an increase in the percentage of late apoptotic cells (31.2 %, $p < 0.05$), compared to the control (Fig. 2B). Additionally, the percentage of necrotic cells increased from ~3 % in the single DNR treatment to 17 % in the combination treatment ($p < 0.01$), compared to the control (Fig. 2B). After increasing the DNR concentration to 1.3 μM, the percentage of late apoptotic cells augmented from ~51 % ($p < 0.01$) in the single DNR treatment to ~78 % ($p < 0.001$) in the combination treatment, compared to the control (Fig. 2B). The apoptotic cell percentage after 1.5 μM DNR treatment was ~73 % ($p < 0.0001$) and after combination with SB203580, the apoptotic cell percentage reached ~92 % ($p < 0.0001$) of the cell population, compared to the control (Fig. 2). In both combination treatments testing DNR at 1.3 and 1.5 μM, the percentages of late apoptotic KG1a cells significantly ($p = 0.012$ and $p = 0.0027$, respectively) increased, compared to the combination treatment with IC_{50} (0.7 μM) DNR (Fig. 2B). Furthermore, the percentage of necrotic cells decreased from 16.5 % ($p < 0.0001$) in the single 1.5 μM DNR treatment to 7.6 % after the combination treatment ($p < 0.01$), compared to the control (Fig. 2B). The negative control 0.2 % DMSO and SB203580 treatment did not affect the high cell viability, compared to the control (Fig. 2).

To confirm DNR-induced apoptosis, the protein expression level of the key enzymes well-known to prompt apoptosis, was assessed using Western blot technology. Thus, the occurrence of apoptosis was verified by detecting the expression levels of cleaved caspase-3, cleaved caspase-9, and cleaved PARP. The results showed a clear detection of those apoptotic markers in KG1a cells treated with 0.9 (IC_{50}) and 1.3 μM DNR for 48 h, compared to the control (Fig. 3). Additionally, when the cells were exposed to SB203580 prior to DNR treatment, a significant ($p < 0.05$) increased detection of each cleaved fragment was observed. Of note, the cleavage of PARP and caspase-9 observed in the combination

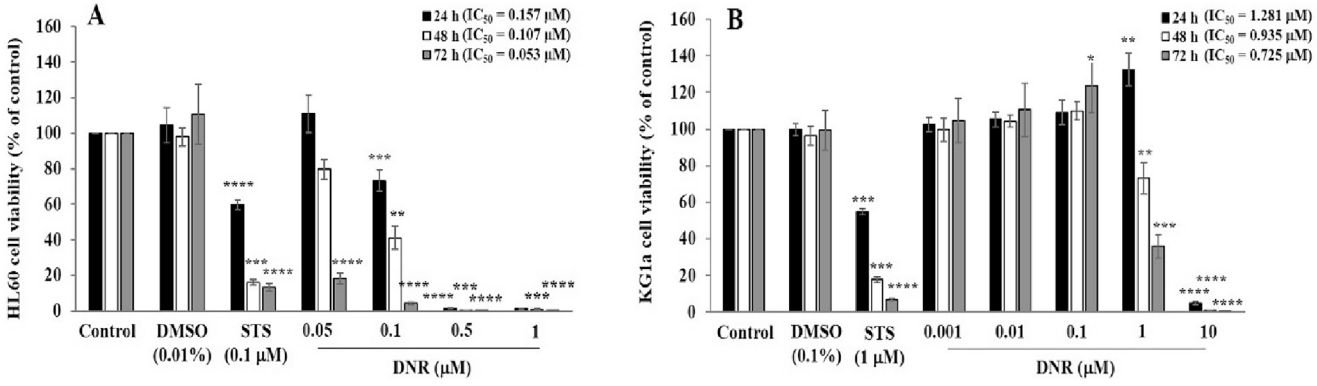

Fig. 1. Chemoresistance potential of KG1a cells in response to DNR, in contrast to the chemosensitive HL60 cells. HL60 (A) and KG1a (B) cells were treated with increasing DNR concentrations for 24, 48, and 72 h. Cell viability was assessed using the CellTiter-Glo® Luminescent Cell Viability Assay and IC_{50} were determined. The results were normalized to the control (100 %) and presented as mean ± SD for three independent experiments. *$p < 0.05$, **$p < 0.01$, ***$p < 0.001$, and ****$p < 0.0001$, compared to the control.

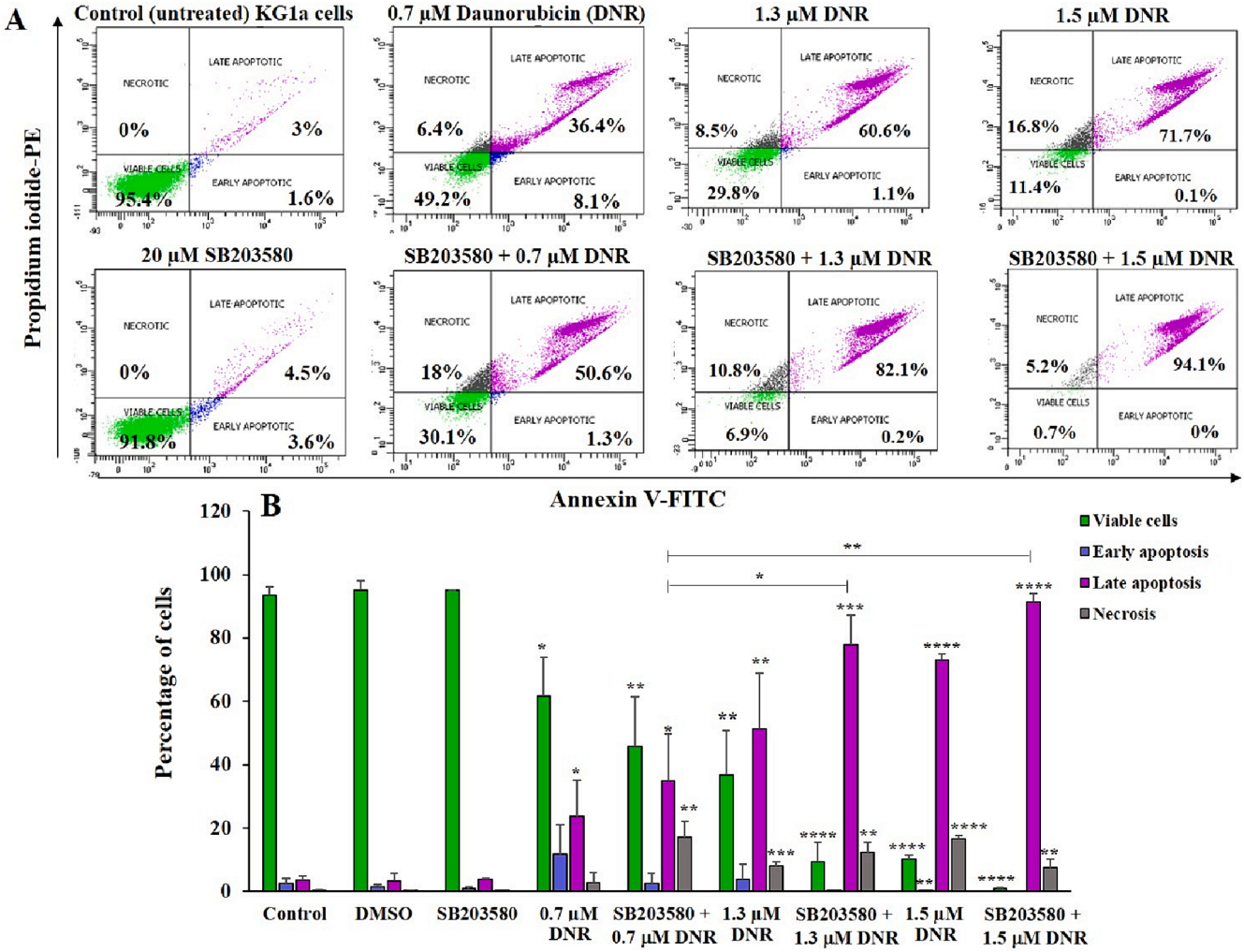

Fig. 2. Apoptosis status determination of KG1a cells exposed to DNR with or without SB203580 pretreatment. (A) Representative flow cytometry scatter plots of KG1a cells treated with 0.7 µM (IC_{50}), 1.3 µM, and 1.5 µM DNR for 72 h with or without SB203580 pretreatment. (B) Bar graph of KG1a cell percentage of the status, determined as viable, apoptosis, and necrosis, presented as mean ± SD for three independent experiments. *$p < 0.05$, **$p < 0.01$, ***$p < 0.001$, and ****$p < 0.0001$, compared to the control.

treatment was accompanied by a significant decrease in full fragment PARP and pro-caspase-9 expression. As expected, none of these cleaved forms were detected in the control group, as well as in the negative control (0.2 % DMSO) and SB203580-treated cells (Fig. 3).

The pro-apoptotic effect of DNR in KG1a cells and the potentiation of its effect after blocking p38 MAPK using SB203580 were visualized using Image-iT™ LIVE kits for evaluation of executioners caspase-3/-7 and intrinsic pathway-related mPTP activities. After 72 h of treatment, the nuclei of KG1a cell were stained with Hoechst 33342, while caspase activity and nucleic acid localization were revealed by red fluorescence and green fluorescence, respectively. Representative photomicrographs show that KG1a cell exposure to 0.7 µM (IC_{50}) DNR and to DNR after SB203580 pretreatment resulted in a significant ($p < 0.001$) 60 % and 70 % decrease in the cell number, compared to DMSO-(100 %) and SB203580-treated cells (Fig. 4A-B). Low caspase activity was observed in DMSO- and SB203580-treated cells, while 20 % of the cell population exhibited caspase activity after DNR addition and 55 % of the cell population underwent caspase activity upon the combination treatment (Fig. 4A and C). Dead cells were indicated by the presence of nucleic acids spread throughout the cells (Fig. 4A). Dead cells were accounted for 30 % of the cell population upon the combined treatment, compared to DMSO-treated cells, while low percentages of dead cells were observed in SB203580 and DNR single treatments (Fig. 4A and C).

Regarding mPTP activity, representative photomicrographs also show similar variations in the nuclei-stained cell number, including more dead cells caused by the combined treatment, compared to DNR cytotoxic effect (Fig. 5A and B). The activity of mPTP was evaluated based on the release of the mitochondrial components, resulting in the quench of green fluorescent calcein (Fig. 5A). Compared to the expected low mPTP activity in healthy viable DMSO- and SB203580-treated cells, a significant ($p < 0.0001$) drastic increase in mPTP activity by 74.5 % and by 85.5 % was observed in DNR and combined treatment, respectively (Fig. 5A and C). The activity of mPTP significantly ($p = 0.029$) increased in the KG1a cells upon combination treatment, compared with the activity assessed in DNR-treated cells (Fig. 5C).

3.3. *Impact of DNR and SB203580 combination treatment on the expression level of signaling and apoptosis-related proteins*

To gain insight into the impact of single DNR treatment and combination (SB203580 + DNR) treatment on protein profiling with respect to signaling and apoptosis, KG1a cell lysates were subjected to human profiler phosphokinase and apoptosis protein arrays. The signaling pathways modulated by DNR alone were first analyzed in comparison with DMSO-treated KG1a cells, the negative control. DNR clearly decreased the phosphorylation of cytoplasmic proline-rich tyrosine

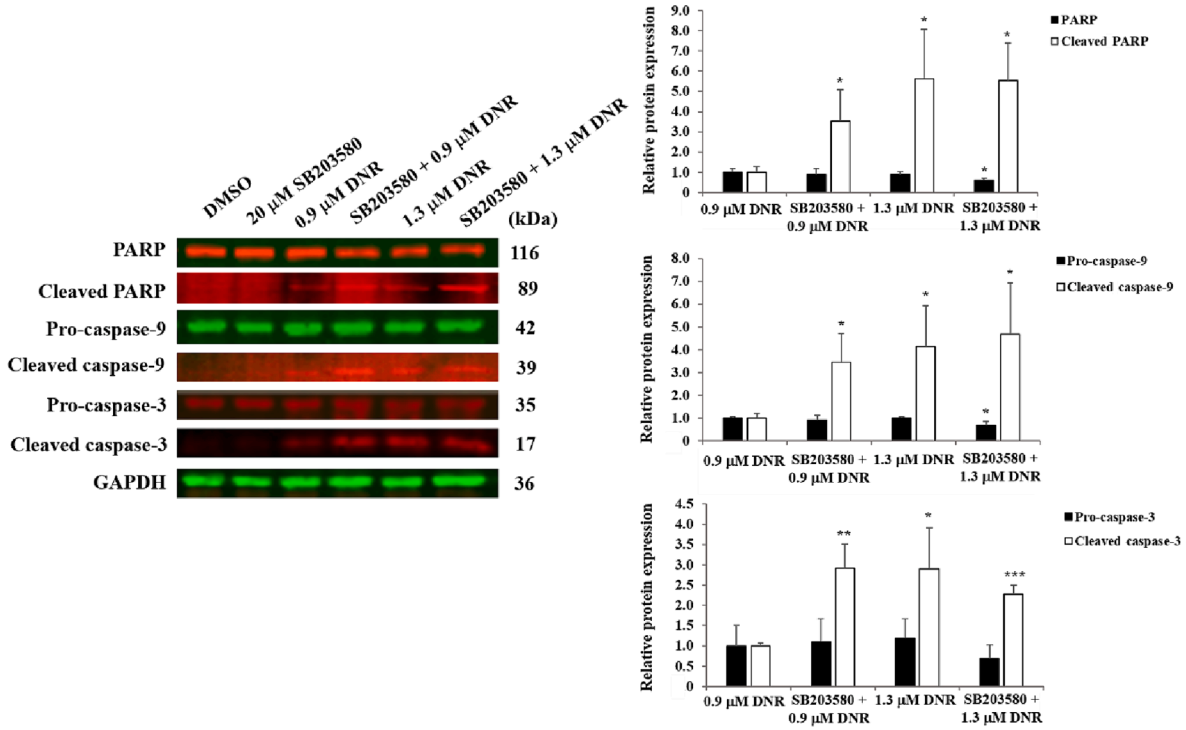

Fig. 3. Detection of cleaved apoptotic proteins in KG1a cells exposed to DNR with or without SB203580 pretreatment. (A) Representative Western blot results showing an increase in the expression levels of cleaved caspase-3, cleaved caspase-9, and cleaved PARP in the SB203580 + DNR-treated cells as compared to the cells treated with DNR alone. (B) Bar graph of quantitative analysis of Western blot using the Image J software. The experiment was repeated three independent times, and presented as mean ± SD. The data was normalized to GAPDH and related to DNR-treated cells. $*p < 0.05$, $**p < 0.01$, $***p < 0.001$, compared to the DNR.

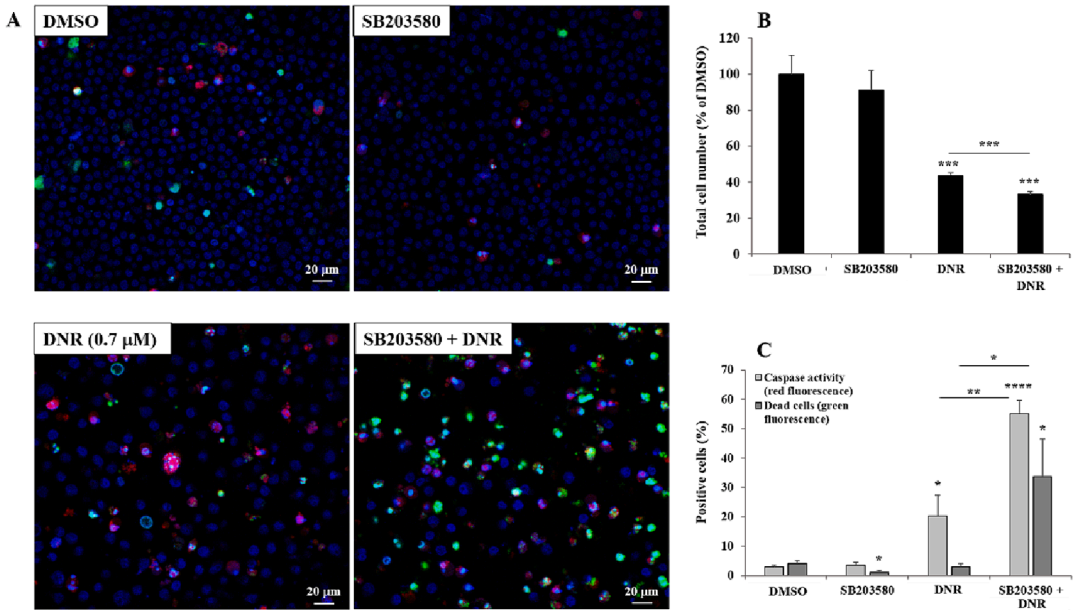

Fig. 4. Potentiation of DNR-induced caspase-3/-7 activity in KG1a cells after SB203580 pretreatment. (A) After 72 h of treatment with the indicated experimental conditions, representative photomicrographs show the nuclei of KG1a cells stained with Hoechst 33,342 (in blue), and fluorescence-based hallmarks of apoptosis revealed by active caspase-3/-7 (visualized in red) and cellular nucleic acids (visualized in green), indicating dead cells. (B) Bar graph of total KG1a cell number expressed in percentage of DMSO-treated cell number. (C) Bar graph of fluorescence-based hallmarks of apoptotic cells positive in red and green fluorescence, indicating caspase activity and dead cells, respectively. The experiment was repeated three independent times, and presented as mean ± SD. $*p < 0.05$, $**p < 0.01$, $***p < 0.001$, and $****p < 0.0001$, compared to the DMSO. (For interpretation of the references to colour in this figure legend, the reader is referred to the web version of this article.)

kinase (PYK), survival-related Akt1/2, p90 ribosomal S6 kinase (RSK)1/2, nuclear cyclic adenosine monophosphate (cAMP) response element-binding (CREB) and signal transducer and activator of transcription (STAT)3 transcription factors, tumor suppressor p53, mitogen- and stress-protein kinase (MSK)1/2, and the expression of heat shock protein (HSP)60, compared to the basal phosphorylation level detected in

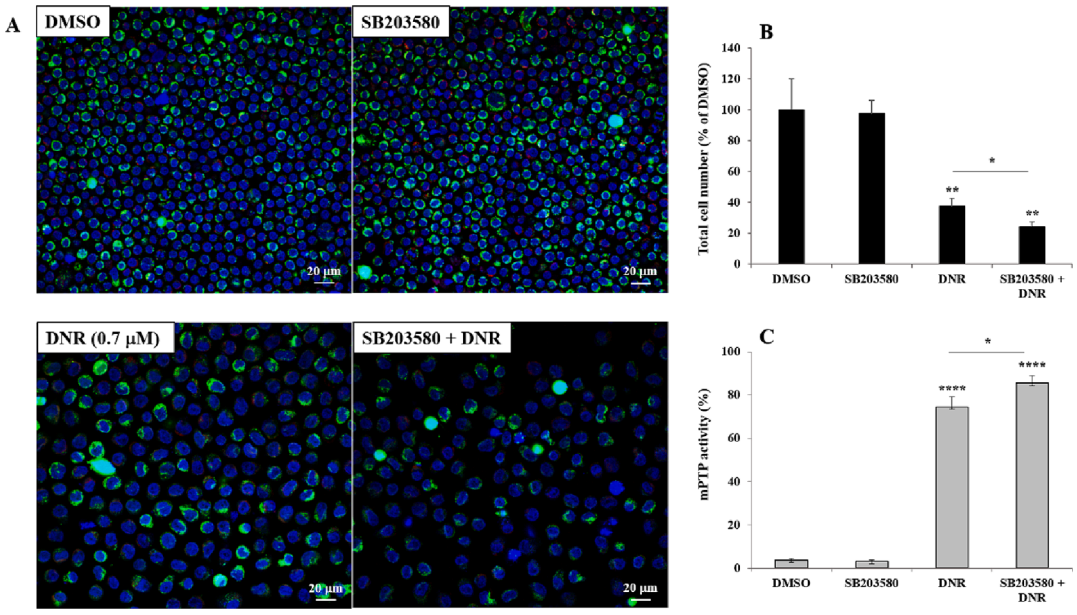

Fig. 5. Increase of DNR-induced mPTP activity in KG1a cells after SB203580 pretreatment. (A) After 72 h of treatment with the indicated experimental conditions, representative photomicrographs (taken at the same magnification) show KG1a cells stained with MitoTracker® Red fluorescence, nucleus dye Hoechst 33,342 (in blue) and green fluorescent calcein/quencher cobalt. (B) Bar graph of total nuclei-stained KG1a cell number expressed in percentage of DMSO-treated cell number. (C) Bar graph of quenched green fluorescence indicating mPTP activity, revealing the release of pro-apoptotic mitochondrial components. The experiment was repeated three independent times, and presented as mean ± SD. $*p < 0.05$, $**p < 0.01$, and $****p < 0.0001$, compared to the DMSO. (For interpretation of the references to colour in this figure legend, the reader is referred to the web version of this article.)

DMSO-treated KG1a cells (Supplementary Fig. 2). In contrast, non-receptor protein tyrosine kinase Yes and STAT5a/b phosphorylation was induced by DNR (Supplementary Fig. 2). In the combination treatment, the phosphorylation of most signaling proteins, including p38 MAPK, was not affected, while an obvious increase in the phosphorylation levels of MSK1/2 (S376/S380), RSK1/2 (S221/S227),

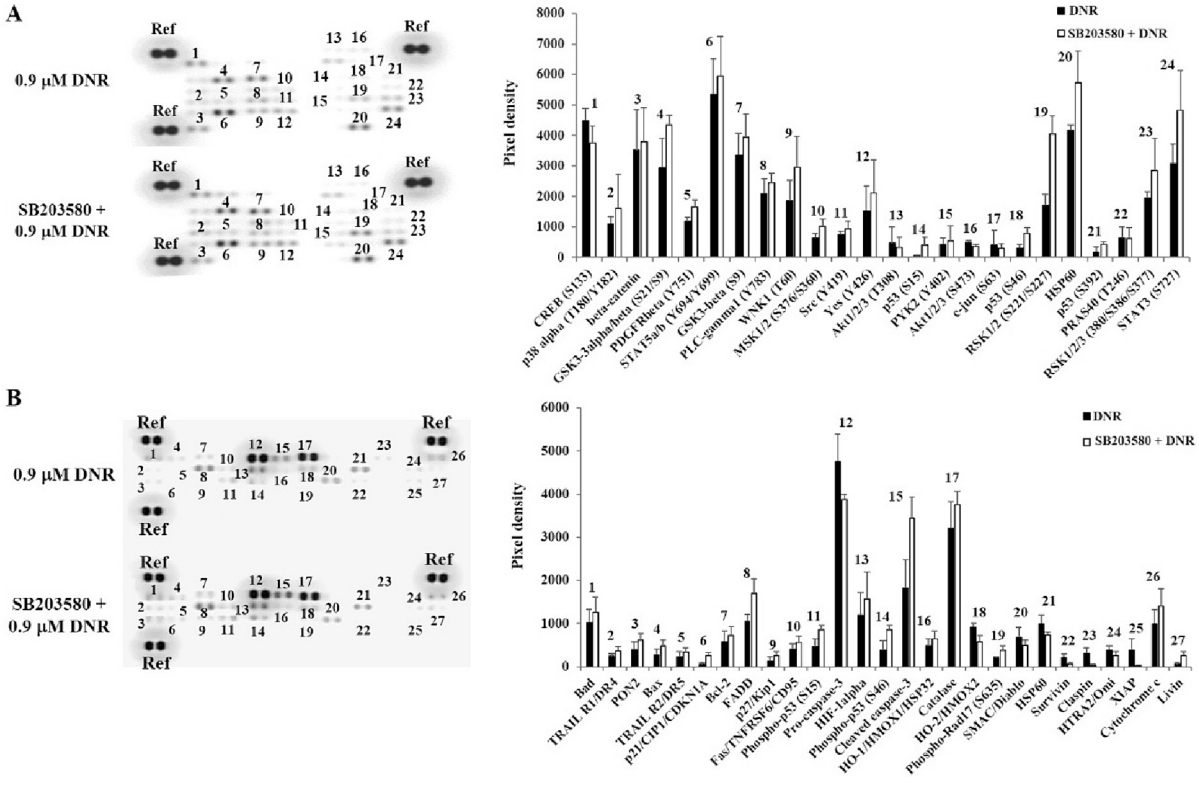

Fig. 6. Analysis of human profiler phosphokinase (A) and apoptosis (B) protein arrays in KG1a cell lysates after 48 h of treatment with either DNR or DNR following SB203580 pretreatment. Representative immunoblots revealing the expression of targeted proteins, indicated in dot blots. Bar graph of quantitative analysis of the blots expressed in pixels using the ImageJ software. The data are presented as mean ± SD for three independent experiments.

STAT3 (S727), and HSP60 was observed, compared to DNR alone (Fig. 6A). As a p38 MAPK inhibitor, SB203580 was reported to block Akt phosphorylation (Wang et al., 2021). Herein, an obvious decrease in Akt 1/2/3 (S473) phosphorylation level was detected in KG1a cells upon the combination treatment, compared to DNR alone (Fig. 6A). Induction of expression or increased expression levels of several isoforms of p53 tumor suppressor protein phosphorylation on S15, S46 and S392 were noticed in KG1a cells upon combination treatment, compared to DNR effect (Fig. 6A). Regarding apoptosis-related proteins, phospho-p53 proteins were also overexpressed in the combination treatment, compared to DNR (Fig. 6B). As a key hallmark of apoptosis, caspase-3 cleavage was revealed by the important increase in cleaved caspase-3 and a concomitant decrease in the expression level of pro-caspase-3 (Fig. 6B). The expression of death receptor-related proteins such as Fas/tumor necrosis factor receptor(TNFR)SF6/CD95, TNF-related apoptosis inducing ligand-receptor (TRAIL-R)1, Fas-associated death domain (FADD) was increased in the combination treatment, compared to DNR alone, as well as the pro-apoptotic mitochondrial proteins (i.e., pro-apoptotic Bad, Bax and cytochrome *c*) whose expression levels were augmented (Fig. 6B). Moreover, the expression levels of most inhibitors of apoptosis proteins (IAPs), such as XIAP, survivin and claspin, were strongly decreased in the KG1a cells upon the combination treatment, compared to DNR alone. Furthermore, a concomitant decrease in the expression level of their antagonist second mitochondria-derived activator of caspases (SMAC)/ direct IAP binding protein with low PI (Diablo) was observed in the combination treatment, compared to DNR (Fig. 6B).

The gene expression level of the main apoptosis-related proteins was monitored using RT-qPCR technology in RNA extracts isolated from untreated (control) KG1a cells and cells treated with DMSO, SB203580, DNR alone or combined treatment SB203580 and DNR. A significant increase in the expression level of the apoptotic tumor suppressor gene *TP53* was noticed in the combined treatment, compared to DNR (Fig. 7A). Additionally, there was a decrease in the expression level of the anti-apoptotic gene *BCL2* in the combination treatment, compared to the DNR effect (Fig. 7A). *Cyclin D1* and *cyclin-dependent kinase inhibitor* (*CDKN)1A* (also known as *p21*), related to cell cycle regulation, also showed drastic changes. In DNR-treated KG1a cells, there was significant upregulation of cyclin D1 mRNA transcript levels by 20.7-fold ($p = 0.0014$) and *CDKN1A* by 53.19-fold ($p = 0.008$), compared to the Control (Fig. 7B). In KG1a cells exposed to the combination treatment, *CDKN1A* mRNA transcript level was further increased, while *cyclin D1* transcript level was slightly decreased compared to the DNR effect (Fig. 7B).

3.4. DNR and SB203580 combination treatment caused KG1a cell growth arrest in S-phase

Analysis of cell cycle progression (sub-G0/G1, G0/G1, S, G2/M) indicates the proliferative state of cells in response to certain chemicals or culture conditions. Therefore, as another cell death mechanism, cell cycle progression was analyzed in KG1a cells exposed to DNR, followed by DNA staining with PI and monitoring of DNA content in percentage of cells using flow cytometry software. Untreated KG1a cells and cells treated with DMSO or SB203580 showed similar profiles, revealed by a negligible percentage of cells in sub-G0/G1 containing apoptotic fragmented DNA, 60–65 % of the cell population in G0/G1, 17 % of cells in S-phase and 15 % of cells in G2/M-phase (Fig. 8A). After 72 h of incubation, DNR treatment resulted in an increase in the percentage of KG1a cells in sub-G0/G1 phase to 10 % and an obvious decrease in the cell percentage in G0/G1-phase reaching 5 % (Fig. 8A). Additionally, no change in the percentage of cells in S-phase was noticed, whereas a drastic increase in the cell percentage in G2/M-phase up to 60 % was observed in DNR-treated KG1a cells (Fig. 8A). Treatment of KG1a cells with SB230580 prior to DNR addition resulted in an increase in the percentage of apoptotic cells (up to 15 %) in sub-G0/G1, a concomitant large increase in the percentage of cells in S-phase reaching 50 % of the cell population followed by 20 % of cells in G2/M-phase (Fig. 8A). Using Western blot analysis, high-molecular-weight of cyclin D1 protein was detected in untreated and treated KG1a cells (Fig. 8B). A significant decrease in high-molecular-weight cyclin D1 level was observed in DNR-treated KG1a cells, compared to the basal expression level detected in untreated cells (Fig. 8B). Unlike cyclin D1 protein expression decreased by DNR, a significant increase in cyclin B1 (2.52-fold, $p = 0.035$) and cyclin A1 (6.42-fold, $p < 0.0001$) was observed in DNR-treated KG1a cells, which was slightly decreased in KG1a cells upon combination treatment, compared to control cells (Fig. 8B).

3.5. Effect of DNR and SB203580 combination treatment on miRNA transcript expression levels in KG1a cells

Playing a major role in AML chemoresistance potential and cancer cell apoptosis induction (Du et al., 2015; Matou-Nasri et al., 2022), the expression level of miR-328-3p and miR-26b-5p transcripts was monitored using RT-qPCR assays. After 48 h of incubation, an upregulation of miR-328-3p transcript (1.95-fold, $p = 0.006$) in KG1a cells treated with DNR IC_{50} (0.9 μM) was observed, compared to untreated (control) and DMSO-treated cells (Fig. 9). In the presence of SB203580, miR-328-3p transcript level tended to increase compared to control and DMSO-treated cells (Fig. 9). Interestingly, there was a further significant upregulation of miR-328-3p (3.6-fold, $p = 0.004$) in SB203580-

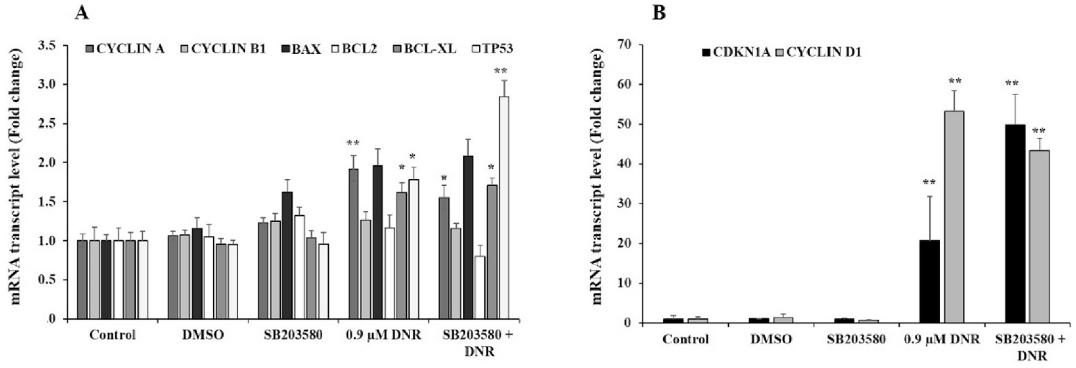

Fig. 7. Variation of mRNA transcript levels of apoptosis and cyclin-related apoptosis in KG1a cells exposed to IC_{50} DNR with or without SB203580 pretreatment. Bar graphs indicating the fold change of (A) cyclins (i.e., *CYCLIN A, CYCLIN B1*), apoptosis-related genes (i.e., *BAX, BCL2, BCL-XL, TP53*), and the fold change of (B) cyclin-dependent kinase CDKN1A and CYCLIN D1, monitored in untreated (i.e., control) and treated KG1a cells using RT-qPCR after 48 h of incubation. The experiment was repeated three independent times, and presented as mean ± SD. The data was normalized to GAPDH and related to DNR-treated cells. *$p < 0.05$ and **$p < 0.01$, compared to the Control.

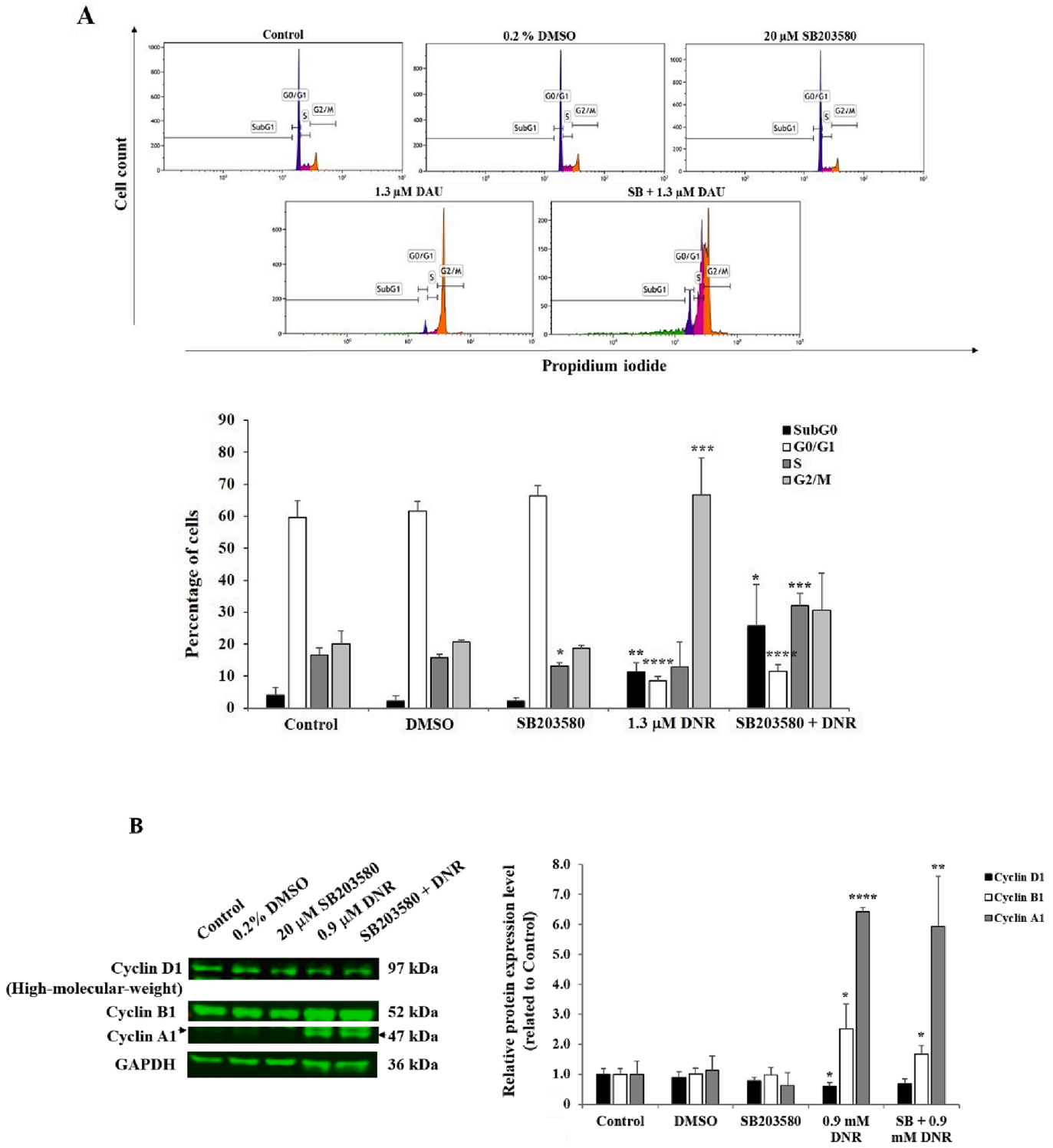

Fig. 8. Cell cycle analysis and detection of cyclin expression levels in KG1a cells after treatment with DNR, with or without SB203580 pretreatment. (A) Representative flow cytometric histograms showing the cell cycle distribution. Bar graph of the cell cycle analysis for three independent experiments presented as mean ± SD. (B) Representative Western blots showing cyclins D1 (high-molecular-weight), A1, B1 expression levels in KG1a cell lysates at the indicated experimental conditions. Bar graph of quantitative analysis of Western blot using ImageJ software. The experiment was repeated three times independently and presented as mean ± SD. The data was normalized to GAPDH and related to the control sample.*$p < 0.05$, **$p < 0.01$, ***$p < 0.001$, and ****$p < 0.0001$, compared to the Control.

pretreated KG1a cells exposed to 0.9 µM DNR, compared to control and DNR ($p = 0.03$) (Fig. 9). Unlike miR-328-3p, no change in miR-26b-5p transcript level was observed under most experimental conditions, but upon the combination treatment, a significant decrease (0.5-fold, $p = 0.019$) was noticed, compared to the basal level monitored in the control untreated cells (Fig. 9).

4. Discussion

Resistance to anthracycline antibiotics such as DNR, hyperactivity of

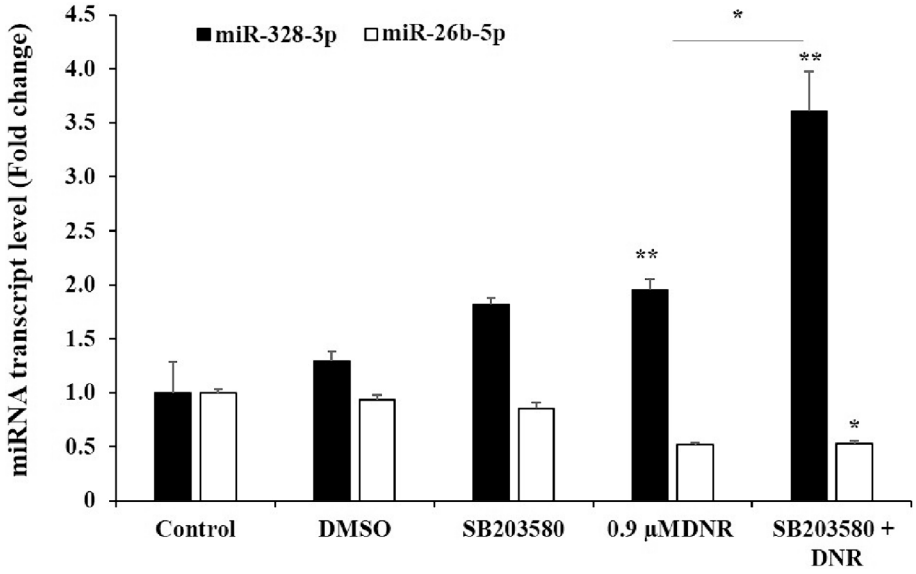

Fig. 9. miRNA transcript levels in KG1a cells after treatment with IC_{50} DNR, with or without cell pretreatment with SB203580. The KG1a cells were treated with 0.9 µM (IC_{50}) DNR for 48 h with or without SB203580 pretreatment. The bar graph shows the fold change of miR-328-3p and miR-26b-5p transcripts determined by RT-qPCR. RT-qPCR fold changes are relative to control samples and normalized to the endogenous control miRNA. The experiment was repeated three times independently and presented as mean ± SD. *$p < 0.05$ and **$p < 0.01$, compared to the control.

survival pathways, and miRNA alteration in AML stem cells are major factors contributing to treatment failure and poor outcome in the patients (Zong et al., 2015; Zhang et al., 2019; Carter et al., 2020; Arwanih et al., 2022; Chandraprabha Vineetha et al., 2024). A reduction in the chemoresistance potential revealed by an enhancement of the apoptosis process undergone by AML stem cells exposed to conventional chemotherapeutic drugs would improve AML patients' health conditions and reduce the relapse rate. Previous studies have shown that p38 MAPK pathway activation is involved in drug resistance with miRNA alterations in many cancers, including AML (Kudaravalli et al., 2022; Yuan et al., 2020), suggesting the crucial role of the p38 MAPK pathway in the chemoresistance potential of KG1a AML stem cells. We previously reported that inhibition of the p38 MAPK pathway by SB202190 enhances the chemosensitivity of KG1a cells to the chemotherapeutic drug 5-Fluorouridine (Matou-Nasri et al., 2022). In this current study, KG1a cell pretreatment with pharmacological p38 inhibitor SB203580 followed by DNR, the suitable chemotherapeutic agent for AML patient, resulted in effective induction of apoptosis, which was investigated extensively, with the analysis of the related signaling pathways, cell cycle profiles, and miRNA expression levels. The pro-apoptotic effect of DNR potentiated by p38 MAPK inhibitor SB203580 pretreatment could contribute to the development of a new combined therapeutic strategy to improve clinical outcomes in patients with refractory or relapsed AML.

The chemoresistance potential of KG1a AML stem cells was confirmed after evaluating cell viability in response to increasing concentrations of DNR and determining IC_{50} values, compared to chemosensitive AML HL60 cells. KG1a cells showed more resistance to the anthracycline DNR than mature HL60 cells. The chemoresistance potential of KG1a cells was characterized by the requirement for higher IC_{50} values of DNR, determined at different incubation times, than those required for HL60 cells. These results are consistent with those of a previous study reporting that immature AML cells were 10- to 15-fold more resistant to DNR than mature cells (Bailly et al, 1995). AML stem cells are well known for the self-renewal, immune evasion and drug resistance, making them as the main leading cause of AML relapse. Thus, various therapeutic strategies targeting AML stem cells and focusing on survival pathways such as p38 MAPK have emerged (Martínez-Limón et al., 2020; Kudaravalli et al., 2022; Li et al., 2023).

Described as playing a key role in chemoresistance and immune evasion, the p38 MAPK pathway has become an interesting therapeutic target to eradicate AML stem cells. In this study, KG1a cells exposed to the pharmacological p38 MAPK inhibitor SB203580 resulted in a slight increase in the cell population undergoing apoptosis. A similar effect was observed after the use of another pharmacological p38 MAPK inhibitor SB202190 (Matou-Nasri et al., 2022). It is noteworthy that both SB203580 and SB202190 inhibit p38 MAP kinase activity through competition with ATP and binding to the ATP-binding pocket, respectively; but in different manners regarding p38 MAPK phosphorylation (Düzgün et al., 2017). These different mechanisms of action were observed by the lack of inhibition of p38α phosphorylation in KG1a cells exposed to SB203580 in this study, while inhibition by SB202190 has been previously reported (Matou-Nasri et al., 2022). Unlike SB202190, SB203580 has been shown to inhibit the phosphorylation of p38β and not p38α (Kuma et al., 2005), suggesting further *in vitro* investigation to better understand the role of each p38 isoform in the survival capacity and chemoresistance of AML stem cells. Furthermore, in this present study, profiling of DNR-modulated signaling pathways in KG1a cells was established by detecting a wide panel of customized targets, including the phosphorylation (activated form) of MAPKs (*i.e.*, p38, ERK, c-jun), p53, Akt, MSK1/2, $p90^{rsk}$. The effectiveness of the p38 MAPK inhibitor SB203580 in KG1a cells was proven by the decreased phosphorylation of Akt, described as a downstream effector of p38 MAPK. The main signaling pathways activated by DNR have been reported to be mediated by $p90^{rsk}$ (Zong et al., 2015). In our current study, the most important signaling protein overphosphorylation induced by DNR after SB203580 pretreatment was found to be on RSK1/2, suggesting deeper investigation into the role of $p90^{rsk}$ in the induction of apoptosis in AML stem cells.

Here, an enhancement of KG1a cell sensitivity to DNR was revealed by an augmented apoptosis induction visualized by flow cytometry after blocking p38 MAPK using the pharmacological inhibitor SB203580, which was greater than our previous study using SB202190 combined with 5-Fluorouridine (Matou-Nasri et al., 2022). Additionally, using *in vitro* and fms-like tyrosine kinase 3 (Flt3)-internal tandem duplication (ITD) and Ten-eleven-translocation 2 (Tet2)-deleted AML genetic mouse models, p38 signaling inhibition in AML cells reduced mesenchymal stem cells-maintained AML chemoresistance potential, which enhanced their sensitivity to the chemotherapy (Anderson et al., 2023). In

addition, In this study, the apoptotic status was confirmed by the detection of apoptosis-related protein markers, such as apoptosis executioner cleaved caspase-3, intrinsic pathway-related cleaved caspase-9, and cleaved PARP for oligonucleosomal DNA fragmentation, and visualized by increased caspase-3/-7 and mPTP activities. All these hallmarks of apoptosis were found to be significantly at higher when SB203580 was combined with DNR than those induced by DNR. Moreover, upregulation of pro-apoptotic tumor suppressor gene *TP53* and downregulation of anti-apoptotic gene *B-cell lymphoma 2* (*BCL)-2* in AML stem cells KG1a upon the combination treatment were observed, compared to the DNR. In agreement with our findings, DNR-induced apoptosis in cancer stem cells was described to be associated with p53 accumulation, caspase cleavage and DNA fragmentation (Seno et al., 2019). Another study reported improved sensitivity to DNR in AML cell lines HL60 and U937 by blocking autophagy through unc-51-like autophagy activating kinase (ULK)1 inhibition (Qui et al., 2020). Thus, further study on the autophagy process induced by DNR after SB203580 pretreatment in AML stem cells could be interesting. Furthermore, using *FLT3/ITD* AML cell lines and xenografts mouse models, a recent study reported the antitumor activity of simvastatin on *FLT3/ITD* AML cells through p38 MAPK inhibition (Li et al., 2023). In the search for novel drugs, many natural products with anti-leukemic activities have also been investigated (Goel et al., 2023), which may be screened for their potential p38 MAPK inhibitory properties in AML stem cells.

Additionally, our results showed that exposure of KG1a cells to DNR altered cell cycle progression. After treating the cells with DNR, KG1a cells were arrested at G2/M-phase, with a subsequent drastic decrease in G0/G1-phase. However, when KG1a cells were exposed to SB203580 before DNR treatment, the cells were arrested in both G2/M- and S-phases. This change in cell cycle progression in KG1a cells caused by DNR and SB203580 combined with DNR was strongly associated with an increase in cyclin B1 and A1 expression patterns and a decrease in cyclin D1. These findings are consistent with the distinct roles of these cyclins, including cyclin B1 playing a key role in controlling G2/M-phase progression, cyclin A1 reported to reach a peak of expression levels in S-phase and G2/M-phase, and cyclin D1 demonstrated to be required for cell cycle progression in G1 (Suski et al., 2021). The cell accumulation in G2/M phase caused by DNR treatment has been mentioned in previous studies (Stojak et al., 2014; Al-Aamri et al., 2019). Stojak et al. (2014) reported G2/M-phase arrest in human AML cell line ML-1 and human acute lymphoblastic leukemia (ALL) cell line MOLT-4 after treating the cells with 50 and 150 nM DNR for 72 h of incubation. Using two acute lymphoblastic leukemia (ALL) cell lines CCRF-CEM and MOLT-4 derived from T lymphocytes, DNR treatment was also reported to cause cell growth arrest in G2/M-phase, accompanied by increased levels of p53 and its target gene cell cycle inhibitor p21 (Al-Aamri et al., 2019; Wang et al., 2021). Both p53 and p21 indicate cell growth arrest and DNA damage due to intercalation of the DNR between DNA base pairs, causing DNA double-strand breaks and topoisomerase II inhibition. In this present study, a drastic upregulation of *TP53* and *p21* (*CDKN1A*) gene expression levels was monitored in KG1a cells upon combination treatment (SB203580 + DNR) compared to DNR stimulatory effects. This enhanced *TP53* and *p21* upregulation was associated with cell growth arrest equally distributed across the apoptotic subG1/G0-phase, DNA replication S-phase and proofread DNA duplication G2/M-phase. Moreover, in a study conducted by Mansilla et al. (2003), Jurkat T cells were exposed to DNR at IC_{50}, which resulted in cell cycle arrest in the G2-phase. However, when tested at IC75, DNR led to cell cycle arrest in G1-phase and immediate apoptosis. These studies highlight the dose-dependent response of DNR on cell cycle progression and the importance of monitoring *TP53, p21* and other apoptosis- and cell cycle-related gene expression levels, which would enhance our knowledge about the mechanism of action of cytotoxic chemotherapeutic drugs. Moreover, in this study, the exact mechanism by which inhibition of the p38 MAPK pathway alters cell cycle distribution after DNR treatment is not well understood. It is possible that the interaction between the signaling pathways affected by the p38 MAPK inhibitor SB203580 and pathways involved in the cellular response to DNR plays a role in this alteration of cell cycle progression. Thus, further research is needed to deeply understand the mechanisms underlying this interaction between the p38 MAPK inhibitor SB203580 and DNR and their impact on more cell cycle-related proteins.

In the present study, the enhancement of KG1a cell sensitivity to DNR after p38 MAPK inhibition, leading to increased apoptosis induction, was associated with concomitant upregulation of the miR-328-3p and slight downregulation of miR-26b-5p. In agreement with our findings regarding downregulation of miR-26b-5p in late apoptotic KG1a cells exposed to DNR with SB203580 pretreatment, downregulation of miR-26b-5p was recently reported to accelerate apoptosis in AML cells (Xie et al., 2024). In addition, using bioinformatics analysis, high levels of miR-26b-5p were associated with poor prognosis in AML and possibly through ubiquitin specific peptidase (USP)48-mediated Wnt/b-catenin molecular axis (Xie et al., 2024). Further research is needed to uncover the molecular pathways causing miR-26b-5p downregulation in KG1a cells exposed to DNR with SB203580 pretreatment. In the present study, upregulation of miR-328-3p in KG1a cells upon combination treatment was observed at a higher extent than that noticed in the previous study using 5-Fluorouridine and SB202190 (Matou-Nasri et al., 2022). In a clinical study conducted by Liu et al. (2015), the detection of low miR-328 expression level in AML patients was associated with aggressive clinicopathological features, as well as poor overall survival and relapse-free survival, compared to AML patients with high miR-328 expression level have a good prognosis, indicating the tumor suppressor role of miR-328 in AML pathogenesis. Several *in vitro* studies using cancer cells transfected with miR-328 mimic showed that miR-328-3p overexpression prompted apoptosis in various cancer cells (Shi et al., 2019; Lu et al., 2021; Wang et al., 2023). While Bai and colleagues (2017) reported the involvement of miR-125a in AML cell resistance to DNR by inhibiting apoptosis; here, we observed that DNR upregulated miR-328-3p expression in AML stem cells KG1a. In addition, miR-328 has been demonstrated to exhibit tumor suppressor effects by altering various signal pathways, including extracellular-signal regulated kinase (ERK), PI3K/Akt, and Wnt signaling pathways (Wang et al., 2023). Therefore, further *in vitro* investigation would be needed to verify whether miR-328-3p could affect p38 MAPK signaling pathway.

5. Conclusions

In the search to overcome AML stem cell chemoresistance to DNR, the crucial chemotherapeutic drug for AML patients, blocking p38 MAPK using pharmacological inhibitor SB203580 resulted in potentiation of DNR-induced apoptosis in KG1a cells, confirmed by further increased in the detection of cleaved caspase-3/-9 and PARP, as well as caspase-3/-7 and mPTP activities as compared to DNR. In addition, p38 MAPK inhibition by SB203580 enhanced DNR-induced *TP53* and *p21* gene expression levels and led to a near-equal cell growth arrest in subG0/G1 apoptotic phase, S-phase, and G2/M-phase while DNR caused cell growth arrest in G2/M-phase. Considered a circulating biomarker of good prognosis in AML patients, remarkable overexpression of miR-328-3p was observed in AML stem cells KG1a upon SB203580 combined treatment with DNR, compared with DNR effect. Overall, these findings could contribute to the development of a new therapeutic strategy by targeting the p38 MAPK pathway using the pharmacological inhibitor SB203580 to improve treatment outcomes in refractory or relapsed AML patients.

Funding

This project was fully funded by King Abdullah International Medical Research Centre (KAIMRC) under grant number RC13/250/R.

CRediT authorship contribution statement

Sara Bahattab: Formal analysis, Methodology, Software, Validation, Visualization, Writing – review & editing. **Ali Assiri:** Data curation, Investigation, Methodology, Validation, Visualization, Writing – review & editing, Writing – original draft. **Yazeid Alhaidan:** . **Thadeo Trivilegio:** Data curation, Formal analysis, Methodology, Software, Validation, Visualization, Writing – review & editing. **Rehab AlRoshody:** Data curation, Formal analysis, Methodology, Supervision, Validation, Visualization, Writing – review & editing. **Sarah Huwaizi:** . **Bader Almuzzaini:** Data curation, Formal analysis, Investigation, Methodology, Supervision, Validation, Visualization, Writing – review & editing. **Abir Alamro:** . **Manal Abudawood:** Investigation, Project administration, Supervision, Writing – review & editing. **Zeyad Alehaideb:** Formal analysis, Investigation, Methodology, Resources, Writing – review & editing. **Sabine Matou-Nasri:** .

Declaration of competing interest

The authors declare that they have no known competing financial interests or personal relationships that could have appeared to influence the work reported in this paper.

Acknowledgements

We would like to thank Mr Hamad Al-Eidi, research technologist at KAIMRC Medical Genomics Research Department, for training Ms Sara Bahattab on the Western blot technology and Dr Mohamed Boudjelal, chairman of KAIMRC Core facility, for the use of the flow cytometer and confocal microscopy.

Appendix A. Supplementary material

Supplementary data to this article can be found online at https://doi.org/10.1016/j.jsps.2024.102055.

References

Al-Aamri, H.M., Ku, H., Irving, H.R., Tucci, J., Meehan-Andrews, T., Bradley, C., 2019. Time dependent response of daunorubicin on cytotoxicity, cell cycle and DNA repair in acute lymphoblastic leukaemia. BMC Cancer 19, 179. https://doi.org/10.1186/s12885-019-5377-y.

Anderson, N.R., Sheth, V., Li, H., Harris, M.W., Qiu, S., Crossman, D.K., et al., 2023. Microenvironmental CXCL12 deletion enhances Flt3-ITD acute myeloid leukemia stem cell response to therapy by reducing p38 MAPK signaling. Leukemia 37, 560–570. https://doi.org/10.1038/s41375-022.01798-5.

Antoon, J.W., Nitzchke, A.M., Martin, E.C., Rhodes, L.V., Nam, S., Wadsworth, S., et al., 2013. Inhibition of p38 mitogen-activated protein kinase alters microRNA expression and reverses epithelial-to-mesenchymal transition. Int. J. Oncol. 42, 1139–1150. https://doi.org/10.3892/ijo.2013.1814.

Arwanih, E.Y., Louisa, M., Rinaldi, I., Wanandi, S.I., 2022. Resistance mechanism of acute myeloid leukemia cells against daunorubicin and cytarabine: a literature review. Cureus 14, e33165, 7759/cureus.33165.

Bai, H., Zhou, L., Wang, C., Xu, X., Jiang, J., Qin, Y., et al., 2017. Involvement of miR-125a in resistance to daunorubicin by inhibiting apoptosis in leukemia cell lines, 1010428317695964 Tumor Biol. 39. https://doi.org/10.1177/1010428317695964.

Boscaro, E., Urbino, I., Catania, F.M., Arrigo, G., Secreto, C., Olivi, M., et al., 2023. Modern risk stratification of acute myeloid leukemia in 2023: Integrating established and emerging prognostic factors. Cancers (Basel) 15, 3512. https://doi.org/10.3390/cancers15133512.

Carter, J.L., Hege, K., Yang, J., Kalpage, H.A., Su, Y., Edwards, H., et al., 2020. Targeting multiple signaling pathways: the new approach to acute myeloid leukemia therapy. Signal Transduct. Target Ther. 5, 288. https://doi.org/10.1038/s41392-020-00361-x.

Chandraprabha Vineetha, R., Anitha Geetha Raj, J., Devipriya, P., Sreelatha, M., Mahitha, M., Hariharan, S., 2024. MicroRNA-based therapies: revolutionizing the treatment of acute myeloid leukemia. Int. J. Lab. Hematol. 46, 33–41. https://doi.org/10.1111/ijlh.14211.

Darici, S., Alkhaldi, H., Horne, G., Jørgensen, H.G., Marmiroli, S., Huang, X., 2020. Targeting PI3K/Akt/mTOR in AML: rationale and clinical evidence. J. Clin. Med. 9, 2934. https://doi.org/10.3390/jcm9092934.

Du, J.Y., Wang, L.F., Wang, Q., Yu, L.D., 2015. miR-26b inhibits proliferation, migration, invasion and apoptosis induction via downregulation of 6-phosphofructo-2-kinase/fructose-2,6-bisphosphatase-3 driven glycolysis in osteosarcoma cells. Oncol. Rep. 33, 1890–1898. https://doi.org/10.3892/or.2015.3797.

Düzgün, Ş.A., Yerlikaya, A., Zeren, S., Bayhan, Z., Okur, E., Boayci, İ., 2017. Differential effects of p38 MAP kinase inhibitors SB203580 and SB202190 on growth and migration of human MDA-MB-231 cancer cell line. Cytotechnology 69, 711–724. https://doi.org/10.1007/s10616-017-0079-2.

Fajardo-Orduña, G.R., Ledesma-Martínez, E., Aguiñiga-Sánchez, I., Mora-García, M.L., Weiss-Steider, B., Santiago-Osorio, E., 2021. Inhibitors of chemoresistance pathways in combination with Ara-C to overcome multidrug resistance in AML. A mini review. Int. J. Mol. Sci. 22, 4955. https://doi.org/10.3390/ijms22094955.

Gabra, M.M., Salmena, L., 2017. microRNAs and acute leukemia chemoresistance: a mechanistic overview. Front Oncol. 7, 255. https://doi.org/10.3389/fonc.2017.00255.

Ganesan, S., Mathews, V., Vyas, N., 2022. Microenvironment and drug resistance in acute myeloid leukemia: Do we know enough? Int. J. Cancer 150, 1401-1411. 1002/ijc.33908.

Goel, H., Kumar, R., Tanwar, P., Upadhyay, T.K., Khan, F., Pandey, P., et al., 2023. Unraveling the therapeutic potential of natural products in the prevention and treatment of leukemia. Biomed. Pharmacother. 160, 114351 https://doi.org/10.1016/j.biopha.2023.114351.

Guo, Y., Wang, W., Sun, H., 2022. A systematic review and meta-analysis on the risk factors of acute myeloid leukemia. Transl. Cancer Res. 11, 796–804. https://doi.org/10.21037/tcr-22-27.

Hou, A.H., Tien, H.F., 2020. Genomic landscape in acute myeloid leukemia and its implications in risk classification and targeted therapies. J. Biomed. Sci. 27, 81. https://doi.org/10.1186/s12929-020-00674-7.

Huang, Y., Zhang, Z., Sui, M., Li, Y., Hu, Y., Zhang, H., et al., 2023. A novel stemness classification in acute myeloid leukemia by the stemness index and the identification of cancer stem cell-related biomarkers. Front Immunol. 14, 1202825. https://doi.org/10.3389/fimmu.2023.1202825.

Isidori, A., Loscocco, F., Curti, A., Amadori, S., Visani, G., 2019. Genomic profiling and predicting treatment response in acute myeloid leukemia. Pharmacogenomics 20, 7. https://doi.org/10.2217/pgs-2018-0202.

Jäger, P., Geyh, S., Twarock, S., Cadeddu, R.P., Rabes, P., Koch, A., et al., 2021. Acute myeloid leukemia-induced functional inhibition of healthy CD34+ hematopoietic stem and progenitor cells. Stem Cells 39, 1270–1284. https://doi.org/10.1002/stem.3387.

Jovein, M.M., Ihorst, G., Duque-Afonso, J., Wäsch, R., Bertz, H., Wehr, C., et al., 2023. Long-term follow-up of patients with acute myeloid leukemia undergoing allogeneic hematopoietic stem cell transplantation after primary induction failure. Blood Cancer J. 13, 179. https://doi.org/10.1038/s41408-023-00953-0.

Khaldoyanidi, S.K., Hindoyan, A., Stein, A., Subklewe, M., 2022. Leukemic stem cells as a target for eliminating acute myeloid leukemia: Gaps in translational research. Crit. Rev. Oncol. Hematol. 175, 103710 https://doi.org/10.1016/j.critrevonc.2022.103710.

Kishtagari, A., Levine, R.L., 2021. The role of somatic mutations in acute myeloid leukemia pathogenesis. Cold Spring Harb. Perspect. Med. 11, a034975 https://doi.org/10.1101/cshperspect.a034975.

Kudaravalli, S., den Hollander, P., Mani, S.A., 2022. Role of p38 MAP kinase in cancer stem cells and metastasis. Oncogene 41, 3177–3185. https://doi.org/10.1038/s41388-022-02329-3.

Kuma, Y., Sabio, G., Bain, J., Shpiro, N., Márquez, R., Cuenda, A., 2005. BIRB796 inhibits all p38 MAPK isoforms in vitro and in vivo. J. Biol. Chem. 280, 19472–19479. https://doi.org/10.1074/jbc.M414221200.

Lei, Z.N., Tian, Q., Teng, Q.X., Wurpel, J.N.D., Zeng, L., Pan, Y., et al., 2023. Understanding and targeting resistance mechanisms in cancer. MedComm (2020) 4, e265. 10.1002/mco2.265.

Levin, M., Stark, M., Ofran, Y., Assaraf, Y.G., 2021. Deciphering molecular mechanisms underlying chemoresistance in relapsed AML patients: towards precision medicine overcoming drug resistance. Cancer Cell Int. 21, 53. https://doi.org/10.1186/s12935-021-01746-w.

Li, G., Yao, J., Lu, Z., Yu, L., Chen, L., Ding, L., et al., 2023. Simvastatin preferentially targets FLT3/ITD acute myeloid leukemia by inhibiting MEK/ERK and p38-MAPK signaling pathways. Drugs Rd. 23, 439–451. https://doi.org/10.1007/s40268-023-00442-6.

Liu, L., Chen, R., Zhang, Y., Fan, W., Xiao, F., Yan, X., 2015. Low expression of circulating microRNA-328 is associated with poor prognosis in patients with acute myeloid leukemia. Diagn. Pathol. 10, 109. https://doi.org/10.1186/s13000-015-0345-6.

Lu, J., Lin, J., Zhou, Y., Ye, K., Fang, C., 2021. MiR-328-3p inhibits lung adenocarcinomagenesis by downregulation PYCR1. Biochem. Biophys. Res. Commun. 550, 99–106. https://doi.org/10.1016/j.bbrc.2021.02.029.

Mansilla, S., Piña, B., Portugal, J., 2003. Daunorubicin-induced variations in gene transcription: commitment to proliferation arrest, senescence and apoptosis. Biochem. J. 372, 703–711. https://doi.org/10.1042/BJ20021950.

Martínez-Limón, A., Joaquin, M., Caballero, M., Posas, F., de Nadal, E., 2020. The p38 pathway: from biology to cancer therapy. Int. J. Mol. Sci. 21, 1913. https://doi.org/10.3390/ijms21061913.

Matou-Nasri, S., Najdi, M., AlSaud, N.A., Alhaidan, Y., Al-Eidi, H., Alatar, G., et al., 2022. Blockade of p38 MAPK overcomes AML stem cell line KG1a resistance to 5-Fluorouridine and the impact on miRNA profiling. PLoS One 17, e0267855.

Miyamoto, T., Sanford, D., Tomuleasa, C., Hsiao, H.H., Olivera, L.J.E., Enjeti, A.K., et al., 2022. Real-world treatment patterns and clinical outcomes in patients with AML unfit for first-line intensive chemotherapy. Leuk Lymphoma 63, 928–938. https://doi.org/10.1080/10428194.2021.20022321.

Nepstad, I., Hatfield, K.J., Grønningsæter, I.S., Reikvam, H., 2020. The PI3K-Akt-mTOR signaling pathway in human acute myeloid leukemia (AML) cells. Int. J. Mol. Sci. 21, 2907. https://doi.org/10.3390/ijms21082907.

Niu, J., Peng, D., Liu, L., 2022. Drug resistance mechanisms of acute myeloid leukemia stem cells. Front Oncol. 12, 896426 https://doi.org/10.3389/fonc.2022.896426.

Récher, C., Röllig, C., Bérard, E., Bertoli, S., Dumas, P.Y., Tavitian, S., et al., 2022. Long-term survival after intensive chemotherapy or hypomethylating agents in AML patients aged 70 years and older: a large patient data set study from European registries. Leukemia 36, 913–922. https://doi.org/10.1038/s41375-021-01425-9.

Seno, A., Mizutani, A., Aizawa, K., Onoue, R., Masuda, J., Ochi, N., et al., 2019. Daunorubicin can eliminate iPS-derived cancer stem cells via ICAD/CAD-independent DNA fragmentation. Cancer Drug Resist. 2, 335-350. 10.20517/cdr.2019.01.

Shi, J., An, G., Guan, Y., Wei, T., Peng, Z., Liang, M., et al., 2019. miR-328-3p mediates the anti-tumor effect in osteosarcoma via directly targeting MMP-16. Cancer Cell Int. 19, 104. https://doi.org/10.1186/s12935-019-0829-7.

Stelmach, P., Trumpp, A., 2023. Leukemic stem cells and therapy resistance in acute myeloid leukemia. Haematologica 108, 353–366. https://doi.org/10.3324/haematol.2022.280800.

Stojak, M., Lukawska, M., Oszczapowicz, I., Opydo-chanek, M., Mazur, L., 2014. Cell-cycle disturbance and induction of programmed death by new formamidine analogs of daunorubicin. Anticancer Res. 34, 7151–7158. PMID: 25503143.

Suski, J.M., Braun, M., Strmiska, V., Sicinski, P., 2021. Targeting cell-cycle machinery in cancer. Cancer Cell 39, 759–778. https://doi.org/10.1016/j.ccell.2021.03.010.

Tiong, I.S., Loo, S., 2023. Targeting measurable residual disease (MRD) in acute myeloid leukemia (AML): moving beyond prognostication. Int. J. Mol. Sci. 24, 4790. https://doi.org/10.3390/ijms24054790.

Trino, S., Laurenzana, I., Lamorte, D., Calice, G., De Stradis, A., Santodirocco, M., et al., 2022. Acute myeloid leukemia cells functionally compromise hematopoietic stem/progenitor cells inhibiting normal hematopoiesis through the release of extracellular vesicles. Front Oncol. 12, 824562 https://doi.org/10.3389/fonc.2022.824562.

Vakiti A, Mewawalla P. Acute myeloid leukemia. [updated 2023 Aug 8]. In: StatPearls [Internet]. Treasure Island (FL): StatPearls Publishing; 2024 Jan-Available from htpps://www.ncbi.nlm.gov/books/NBK507875.

van Gils, N., Denkers, F., Smit, L., 2021. Escape from treatment; the different faces of leukemic stem cells and therapy resistance in acute myeloid leukemia. Front Oncol. 11, 659253 https://doi.org/10.3389/fonc.2021.659253.

Wang, Y., Hou, H., Liang, Z., Chen, X., Lian, X., Yang, J., et al., 2021. P38 MAPK/AKT signalling is involved in IL-33-mediated anti-apoptosis in childhood acute lymphoblastic leukaemia blast cells. Ann. Med. 53, 1461–1469. https://doi.org/10.1080/07853890.2021.1970217.

Wang, H., Xiao, X., Xiao, Q., Lu, Y., Wu, Y., 2020. The efficacy and safety of daunorubicin versus idarubicin combined with cytarabine for induction therapy in acute myeloid leukemia: a meta-analysis of randomized clinical trials. Medicine (baltimore) 99, e20094.

Wang, Z., Xie, W., Guan, H., 2023. The diagnostic, prognostic role and molecular mechanism of miR-328 in human cancer. Biomed Pharmacother. 157, 114031 https://doi.org/10.1016/j.biopha.2022.114031.

Xie, Y., Tan, L., Li, D., Li, C., 2024. miR-26b-5p affects the progression of acute myeloid leukemia by regulating the USP48-mediated Wnt/b-catenin pathway. Crit. Rev. Eukaryot. Gene Expr. 34, 33–44. https://doi.org/10.1615/CritRevEukaryotGeneExpr.2024049380.

Yuan, B., El Dana, F., Ly, S., Yan, Y., Ruvolo, V., Shpall, E.J., et al., 2020. Bone marrow stromal cells induce an ALDH+ stem cell-like phenotype and enhance therapy resistance in AML through a TGF-β-p38-ALDH2 pathway. PLoS One 15, e0242809.

Zhang, J., Gu, Y., Chen, B., 2019. Mechanisms of drug resistance in acute myeloid leukemia. Onco Targets Ther. 12, 1937–1945. https://doi.org/10.2147/OTT.S191621.

Zong, H., Gozman, A., Caldas-Lopes, E., Taldone, T., Sturgill, E., Brennan, S., et al., 2015. A hyperactive signalosome in acute myeloid leukemia drives addiction to a tumor-specific Hsp90 species. Cell Rep. 13, 2159–2173. https://doi.org/10.1016/j.celrep.2015.10.073.